Bioorganic & Medicinal Chemistry Letters xxx (2018) xxx–xxx

Contents lists available at ScienceDirect

Bioorganic & Medicinal Chemistry Letters

journal homepage: www.elsevier.com/locate/bmcl

Utilizing a structure-based docking approach to develop potent G protein-coupled receptor kinase (GRK) 2 and 5 inhibitors

Helen V. Waldschmidt [a,c], Renee Bouley [b], Paul D. Kirchhoff [c], Pil Lee [c], John J.G. Tesmer [a,b,d], Scott D. Larsen [a,c,*]

[a] Department of Medicinal Chemistry, College of Pharmacy, University of Michigan, Ann Arbor, MI, United States
[b] Department of Pharmacology and the Life Sciences Institute, University of Michigan, Ann Arbor, MI, United States
[c] Vahlteich Medicinal Chemistry Core, College of Pharmacy, University of Michigan, Ann Arbor, MI, United States
[d] Department of Biological Sciences, Purdue University, West Lafayette, IN, United States

ARTICLE INFO

Article history:
Received 11 January 2018
Revised 7 March 2018
Accepted 28 March 2018
Available online xxxx

Keywords:
GRKs
Kinases
Docking
GPCRs
Crystallography

ABSTRACT

G protein-coupled receptor (GPCR) kinases (GRKs) regulate the desensitization and internalization of GPCRs. Two of these, GRK2 and GRK5, are upregulated in heart failure and are promising targets for heart failure treatment. Although there have been several reports of potent and selective inhibitors of GRK2 there are few for GRK5. Herein, we describe a ligand docking approach utilizing the crystal structures of the GRK2–Gβγ·GSK180736A and GRK5·CCG215022 complexes to search for amide substituents predicted to confer GRK2 and/or GRK5 potency and selectivity. From this campaign, we successfully generated two new potent GRK5 inhibitors, although neither exhibited selectivity over GRK2.

G protein-coupled receptor (GPCR) kinases (GRKs) regulate the largest class of membrane receptors in the human genome via phosphorylation of receptor C-terminal tails or cytoplasmic loops, and are also implicated in several disease states.[1,2] During heart failure, levels of GRK2 and GRK5 are elevated in many tissues.[3–5] In the heart, this upregulation leads to increased desensitization and uncoupling of the GPCRs located in the heart such as the β-adrenergic and angiotensin II receptors, which regulate contractility and blood flow to the body, respectively.[6,7] Knockdown of either GRK2 or GRK5 in mice subjected to transverse aortic constriction showed cardio-protective effects.[8,9]

GRK2 and GRK5 also affect non-GPCR pathways that further mediate stress responses in the heart.[10–13] GRK2 influences cardiac glucose uptake leading to abnormal cardiac metabolism when upregulated, altering the growth of new cardiomyocytes.[10] Uniquely, GRK5 is the only GRK known to be targeted to the cell nuclei of cardiomyocytes[14,15] where it acts as a histone deacetylase (HDAC) kinase.[11] Phosphorylation of HDAC5 leads to increased expression of myocyte enhancer factor-2 which regulates the stress response in hypertrophy.[16,17] Due to these GPCR-independent roles, GRK2 and GRK5 represent promising targets that offer unique therapeutic outcomes that cannot be attained by current heart failure treatments that directly target GPCRs or angiotensin-converting enzyme.

GRK2 and GRK5 have also been implicated in other medical conditions. Elevated levels of cytosolic GRK2/5 have been implicated in Alzheimer's and Parkinson's disease.[18–20] GRK5 has additionally been shown to regulate tumor growth progression in several cancers.[20–23] Also of considerable interest are the roles of GRK2 and GRK5 in cell growth and insulin levels leading to diabetes.[24,25] Thus, chemical probes targeting either GRK2 or GRK5 (or potentially both), would be useful as tools to investigate the roles of GRK2 and GRK5 in cells and human disease.

There are several reported GRK2 and GRK5 inhibitors (Fig. 1). Compound **1o** has a GRK2 IC_{50} of 460 nM but is ~10-fold more potent for GRK5 (IC_{50} of 59 nM).[26] Thus it is one of the most potent GRK5 inhibitors reported to date and one of the few that exhibits some selectivity for GRK5 over GRK2. Limiting its usefulness is its ability to inhibit tyrosine kinases (IC_{50} for c-Met, 8 nM and IC_{50} for anaplastic lymphoma kinase, 0.3 μM).[26,27] Previously, our lab identified compound **GSK180736A** as a GRK2-selective inhibitor. Further development of this scaffold led us to **CCG215022**, which potently inhibits both GRK2 and 5 (Fig. 1).[12,13]

The parent compound **GSK180736A** was co-crystallized with GRK2–Gβγ (PDB entry 4PNK)[28] whereas **CCG215022** was co-crystallized with GRK5 (PDB entry 4WNK), allowing the use of

* Corresponding author at: Department of Medicinal Chemistry, College of Pharmacy, University of Michigan, Ann Arbor, MI, United States.
E-mail address: sdlarsen@umich.edu (S.D. Larsen).

https://doi.org/10.1016/j.bmcl.2018.03.082
0960-894X/

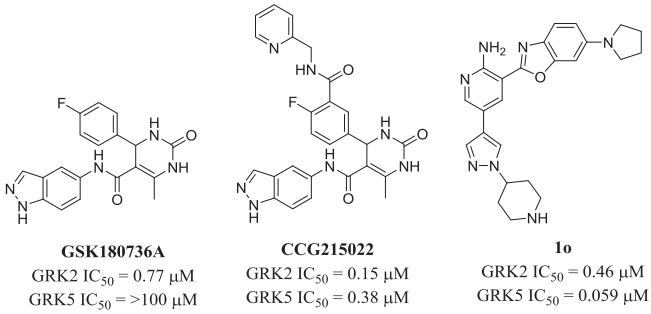

Fig. 1. Reported small molecule GRK inhibitors. GSK180736A and CCG215022 were previously reported by our lab using a radioactivity assay. Compound 1o was reported by Cho et. al. and its IC_{50} values were determined using a time-resolved fluorescence resonance energy transfer assay. Due to different assay conditions the values may not be directly comparable.

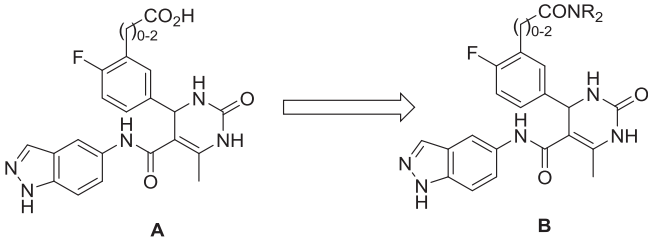

Fig. 3. Virtual library of amides generated from GSK180736A carboxylic acid homologs.

structure-guided drug design to develop potent GRK5 inhibitors.[29] The two compounds bind similarly in the kinase active sites of GRK2 and GRK5, respectively (Fig. 2). The indazole forms two hydrogen bonds to backbone atoms in the hinge of the kinase, the dihydropyrimidinone sits in the ribose subsite, and the fluorophenyl ring packs under the P-loop. The amide-linked pyridine extension of **CCG215022** forms additional hydrogen bonds via its amide with the P-loop and via the pyridine nitrogen with Lys220 and Asp329.[28,29] We hypothesized that we could use these two crystal structures and molecular modeling to design new compounds *in silico* with improved selectivity and potency for either GRK2 or GRK5.

Enumeration of virtual compounds and docking of those compounds was conducted using the computational chemistry package MOE.[30] Our campaign began with an extensive virtual screen using a library of commercially available amines from Sigma Aldrich. Virtual compounds (amides **B**, Fig. 3) were enumerated based on the **GSK180736A** template bearing homologous carboxylic acids off the fluorophenyl ring (**A)** (Fig. 3). The three acid scaffolds **A** were combined with primary and secondary amines (R_2NH) with molecular weights less than 215 g/mol. Initially nearly 15,000 amine structures were retrieved. After removal of amines containing expected reactive or mutagenic chemical motifs by MOE, the number of structures dropped to just over 11,000. The resulting amide compounds **B** were then filtered by a molecular-weight cut off of 550 to give 9183 virtual unique amide-linked structures. We chose a slightly higher molecular weight cut-off of 550 to allow for more diversity of appendages in our larger ethylene linked scaffold which already had a molecular weight of 437 g/mol.

A pharmacophore model was generated based on the ligand orientations in the GRK2–Gβγ·**GSK180736A** and GRK5·**CCG215022** crystal structures. The model restricted the docked ligands to be in an orientation similar to what was seen in the respective crystal structures. As represented in Fig. 4, the center of the indazole and the fluorophenyl rings were constrained by a spherical volume indicated by the green circles in Fig. 4 (radii: 1.8 Å for the indazole rings and 2.5 Å for the fluorophenyl). The two nitrogens of the indazole that form hydrogen bonds with the hinge of the kinase domain were constrained to a spherical volume with a radii of 1.8 Å (purple and cyan circles in Fig. 4). The goal was to allow these motifs to move within a constrained volume of the active site such that new amide substituents would necessarily be projected into the hydrophobic subsite where they could pick up additional interactions to increase potency of the molecules.

The virtual compounds were then docked into ligand-free crystal structures of GRK2–Gβγ and GRK5 using a rigid model of the protein and a flexible ligand model that obeyed the constraints of the pharmacophore model. The results were sorted by highest docking scores (S), where a lower number correlates with tighter binding, and then further divided into three groups. The first group contained compounds predicted to be both potent and selective for GRK2 (S score for GRK2 2 units lower than that of GRK5). The second group contained compounds that were predicted to be both potent and selective for GRK5 (S score for GRK5 2 units lower than that of GRK2). The third group encompasses compounds that were predicted to be equipotent for both GRK2 and GRK5 (having S scores within 2 units of each other) and that had good docking scores. After filtering out any diamines, carboxylic acids, or other reactive, unstable, or toxic motifs that were missed in the

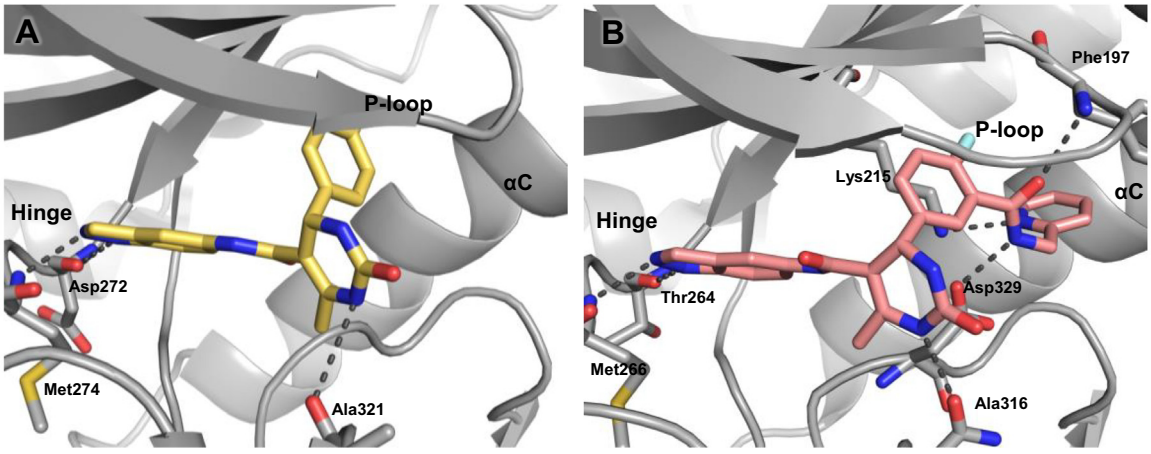

Fig. 2. Comparison of the A) GRK2–Gβγ·GSK180736A (4PNK) and B) GRK5·CCG215022 (4WNK) crystal structures utilized in the docking campaign. GSK180736A is drawn with yellow carbons, CCG215022 is drawn with salmon carbons, and H-bonds are shown as dark grey dashed lines.

Please cite this article in press as: Waldschmidt H.V., et al. Bioorg. Med. Chem. Lett. (2018), https://doi.org/10.1016/j.bmcl.2018.03.082

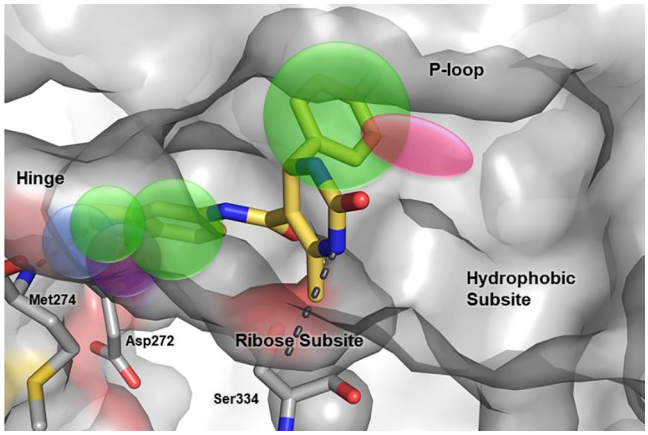

Fig. 4. Pharmacophore model used for molecular docking. GRK2–Gβγ·GSK180736A crystal structure. The green circles represent regions in which the aromatic rings were confined. The cyan and purple circles represent the hydrogen bonds made between the indazole and the backbone of the hinge in the GRK2 and 5 kinase domains. The nitrogens of the indazole were confined to these spheres. The pink oval shows the position where virtual amides were appended and allowed to freely extend into the hydrophobic subsite.

automated filter previously run in MOE, the forty highest scoring virtual amides were synthesized and tested for kinase activity to evaluate the predictive value of this docking approach.

New amides were prepared as previously described for direct amide-linked appendages (n = 0)[13] (Scheme 1). Treatment of 5-aminoindazole **1** with 2,2,6-trimethyl-4*H*-1,3-dioxin-4-one resulted in the acetylated compound **2**.[31] Through a Biginelli cyclization, catalyzed by ytterbium triflate, acids **3**–**5** (synthesis of **3** and **4** are previously reported[13] and synthesis of **5** is shown below) were condensed with urea and acetamide **2** to yield the dihydropyrimidones **6**–**8**.[32] Derivatives were then introduced via amidation resulting in the final compounds **9**–**48**.

The propanoic acid intermediate **5** was synthesized as shown in Scheme 2 beginning with TBS protection of (4-fluorophenyl) methanol **49** to give intermediate **50**. Directed lithiation followed by formylation gave the aldehyde **51**, which was then deprotected to furnish alcohol **52**. Condensation with malonic acid followed by hydrogenation of the resulting alkene gave acid **54**. Parikh-Doering oxidation of the benzylic alcohol cleanly provided aldehyde **5**.

Biochemical evaluation of these compounds was performed using phosphorylation assays against GRK1, 2, and 5, representing the three major GRK subfamilies, as previously described.[33]

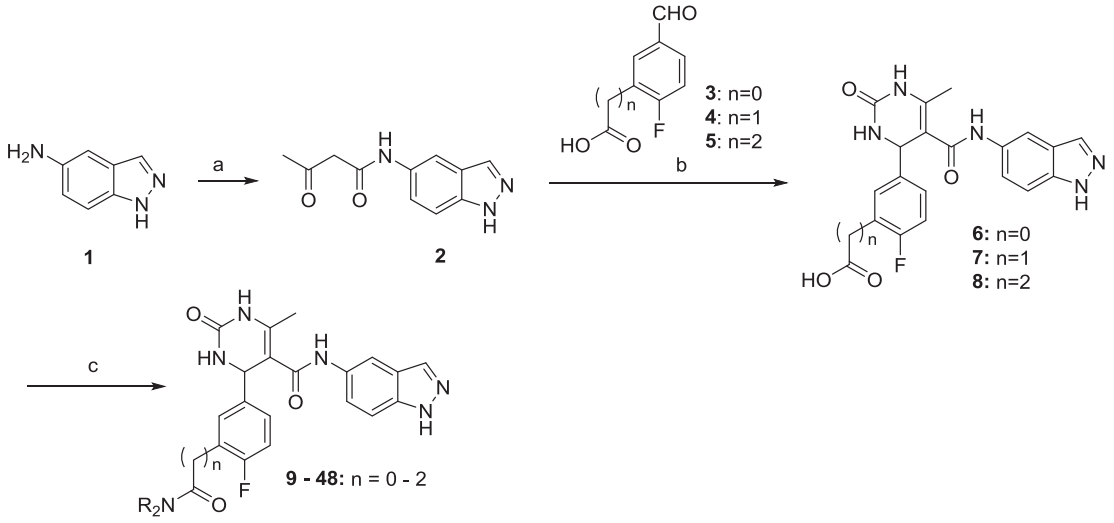

Scheme 1. Preparation of new amides. Reagents and conditions: a) 2,2,6-trimethyl-4H-1,3-dioxin-4-one, CH_3CN, 100 °C, 16 h, 69% b) **3**, **4**, or **5**, and $Yb(OTf)_3$, urea, CH_3CN, 100 °C, 4 h, 63–84% c) HATU, DIEA, R_2NH, DMF, 16 h, 5%–85%.

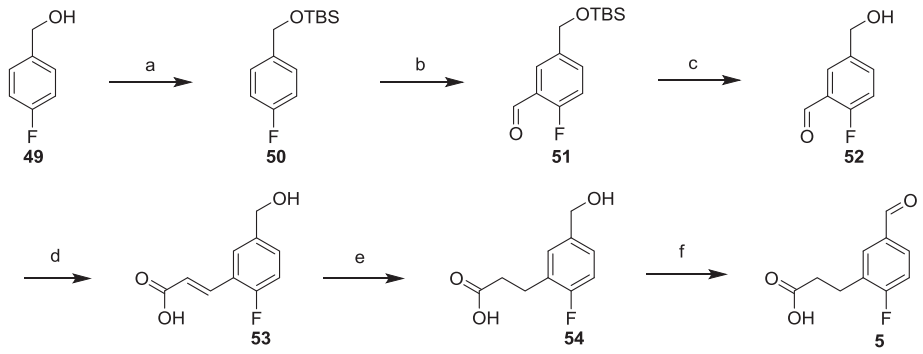

Scheme 2. Synthesis of propanoic acid intermediate **5**. a) TBSCl, imidazole, DIEA, DCM, 12 h, 74%, b) sBuLi, TMEDA, THF, −78 °C then DMF, rt, 3 h, 77%, c) TBAF, THF, 6 h, 74%, d) Malonic acid, pyridine, piperidine, 100 °C, 4 h, 80%, e) 10% Pd/C, H_2, EtOAc, 24 h, 91%, f) SO_3-pyridine, DMSO, Et_3N, 20 min, 79%.

Please cite this article in press as: Waldschmidt H.V., et al. Bioorg. Med. Chem. Lett. (2018), https://doi.org/10.1016/j.bmcl.2018.03.082

The compounds ranged dramatically in terms of both potency and selectivity from the sub-μM to high μM range. The results of the top forty ranked compounds in terms of their activity against GRKs 1, 2, and 5 as well as their GRK2 and GRK5 docking scores (S) are summarized in Tables 1–3. Of the forty hybrid compounds that were docked, synthesized, and tested, 23 (57.5%) showed the predicted selectivity and potency. In evaluating these compounds, we divided them into those that were predicted to be GRK2 selective and/or potent (Table 1), those that were predicted to be GRK5 selective and/or potent (Table 2), and those that were predicted to be similarly potent for both GRK2 and GRK5 (Table 3).

Compounds predicted to be GRK2 selective and/or potent are ordered in Table 1 from the predicted lowest to highest binding affinity based on their docking scores (S). As a whole, the amide substituents in this group were the bulkiest and most conformationally restricted of the three sets, consistent with the previously observed structure-activity relationship (SAR) trend we reported wherein the size and shape of the hydrophobic subsite heavily influences GRK selectivity.[13] GRK2 has a larger and shallower subsite pocket in comparison to GRK5, allowing bulkier D-ring substituents to selectively bind GRK2.[13] Overall, the direct amide-linked analogues (n = 0) all bound with sub-μM potency except for the *N*-methyl analog (**14**) which contains a tertiary amide and thus loses its ability to accept a hydrogen bond from the P-loop. The direct amide-linked compounds all retained selectivity for GRK2 over GRK5 (averaging 22-fold) with the least selective analog being the imidazo pyridine **16** (3.5-fold). Although the imidazo substituent is bulky, it may retain low micromolar potency (GRK5 IC_{50} = 1.9 μM) because of similarities of its substituent nitrogen to that of **CCG215022**. Of the other two core scaffolds (n = 1 and n = 2), all but the 5-methyl isoindoline **9** showed reduced potency against GRK2 compared to the parent **GSK180736A** compound.

There were only five compounds that were predicted to be GRK5 selective and/or potent, which may reflect the fact that the smaller hydrophobic pocket in GRK5 makes it more difficult to accommodate a broad array of D-ring substituents (sorted by GRK5 S score in Table 2). Four of the five compounds had an n = 1 linker, and one had an n = 2 linker. All were, however, selective for GRK2 over GRK5 (10 – 28-fold) with the most GRK2 potent compound being the cyclopropylpiperidine analog **27** (GRK2 IC_{50} = 0.68 μM) and the most GRK5 potent compounds being **27** and the imidazole analog **29** (both with an IC_{50} of 19 μM).

Table 1
GRK activity of indazole-dihydropyrimidinone based compounds predicted to be GRK2 selective and potent.

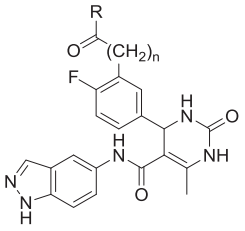

Compound	R	n	GRK2 (IC_{50} μM)	GRK1 (IC_{50} μM)	GRK5 (IC_{50} μM)	GRK2 S	GRK5 S
9		1	0.20 ± 0.06	>100	6.3 ± 1.5	−7.9	−2.2
10	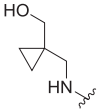	2	3.8 ± 1	>100	>100	−8.2	ND
11	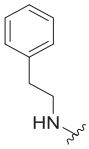	2	4.7 ± 3	>100	>100	−8.3	−5.1
12	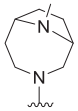	1	2.1 ± 2	>100	6.1 ± 2.7	−8.4	−5.9
13	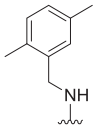	1	1.9 ± 0.6	>100	>100	−8.4	−4.3
14	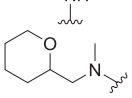	0	14 ± 2	>100	>100	−8.6	−6.6

Table 1 (*continued*)

Compound	R	n	GRK2 (IC_{50} μM)	GRK1 (IC_{50} μM)	GRK5 (IC_{50} μM)	GRK2 S	GRK5 S
15	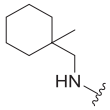	2	1.8 ± 0.4	>100	>100	−8.6	−2.7
16	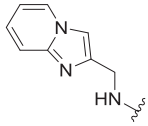	0	0.54 ± 0.06	17 ± 3	1.9 ± 0.6	−8.7	ND
17	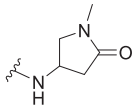	1	1.9 ± 0.3	>100	27 ± 13	−8.8	ND
18	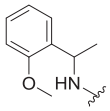	0	0.40 ± 0.1	16 ± 4.4	2.8 ± 0.6	−8.9	−5.9
19	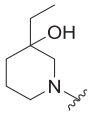	2	29 ± 30	>100	>100	−9.0	−6.0
20	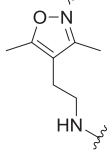	0	0.64 ± 0.08	>100	18 ± 12	−9.1	−6.3
21	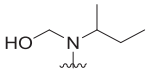	1	1.9 ± 0.2	>100	38 ± 13	−9.1	−6.2
22	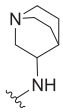	0	0.50 ± 0.08	>100	21 ± 6	−9.2	−5.0
23	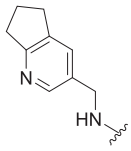	0	0.34 ± 0.03	>100	9.5 ± 0.18	−9.2	ND
24		0	44 ± 12	>100	>100	−9.5	−7.5
25	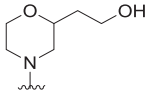	1	1.5 ± 0.4	>100	12 ± 2	−9.6	−7.4

[*] All IC_{50} measurements are an average of three separate experiments run in duplicate. Errors shown represent standard error of the mean. S is the docking score generated by MOE. ND stands for "not docked" as MOE was unable to fit the motif into the pocket according to the restrictions given.

The third set of compounds evaluated were those that were predicted to be potent inhibitors of both GRK2 and GRK5. These eighteen compounds are shown in Table 3 sorted by their predicted binding potentials (weakest to tightest) for either GRK2 or GRK5. A wide variety of appendages were predicted to bind well to both GRK2 and GRK5, including bulky lipophilic substituents, smaller lipophilic substituents, and various heterocycles. The bulkier lipophilic appendages as well as the smaller lipophilic substituents (**31**, **32**, **36**, **38**, **39**, **41**, **42**, **44**, **46**, **47**, and **48**) all exhibited GRK2 selectivity and very poor binding to GRK5 (no sub-μM IC_{50} values). The cyclohexyl methyl ester analog (**45**), which exhibited some lipophilicity via its cyclohexyl and some polarity via its methyl ester, had the best GRK2 IC_{50} (0.16 μM), and was 120-fold selective over GRK5.

All five heterocyclic compounds from this set bound to both GRK2 and GRK5 with potencies lower than 5 μM with the exception of the pyrazole **40**. Two of these heterocyclic compounds bound nearly equipotently to GRK2 and GRK5: the oxadiazoles **37** (GRK2 IC_{50} = 0.16 μM, GRK5 IC_{50} = 0.38 μM) and **33** (GRK2 IC_{50} = 0.25 μM, GRK5 IC_{50}s = 0.26 μM). Moving forward it may be advantageous to expand upon these results by investigating a broader range of small heterocyclic appendages.

To better understand the molecular basis for how the equipotent GRK2/GRK5 inhibitor **33** exhibits improved potency against GRK2, the crystal structure of **33** in complex with GRK2–Gβγ was determined using conditions described previously (PDB: 6C2Y).[12] The inhibitor binds analogously to our previously reported **GSK180736A**-based GRK2 inhibitors (Fig. 5A)[13] and in accordance

Table 2
GRK activity of indazole-dihydropyrimidinone based compounds predicted to be GRK5 selective and potent.

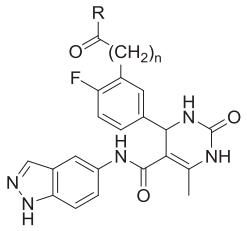

Compound	R	n	GRK2 (IC_{50} μM)	GRK1 (IC_{50} μM)	GRK5 (IC_{50} μM)	GRK2 S	GRK5 S
26	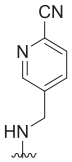	1	1.4 ± 0.3	>100	27 ± 6	−7.2	−9.2
27	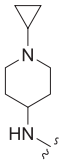	1	0.68 ± 0.04	>100	19 ± 10	−7.1	−9.4
28	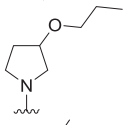	1	1.6 ± 0.09	>100	25 ± 9	−8.1	−10.2
29	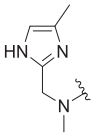	1	2.0 ± 0.3	>100	19 ± 10	−7.7	−10.2
30	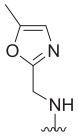	2	4.0 ± 0.5	>100	66 ± 9	−8.3	−10.7

*All IC_{50} measurements are an average of three separate experiments run in duplicate. Errors shown represent standard error of the mean. S is the docking score generated by MOE.

with the pharmacophore model utilized in the docking campaign. The carbonyl of the amide linker forms an additional hydrogen bond with the backbone nitrogen of Phe202. The oxadiazole ether then packs back into the hydrophobic pocket with the oxygen facing the solvent exposed region of the active site.

Comparison of the GRK2–Gβγ·**33** crystal complex with the initial, best scored docking pose of **33** bound to GRK2 (Fig. 5B) revealed, however, that the docking algorithm was unable to correctly model the oxadiazole ether appendage in the hydrophobic subsite. This discrepancy is likely due to the fact that the protein was kept rigid during docking. For example, the crystal structure shows up to a 2.6 Å shift of the P-loop (at the Phe202 Cα carbon) relative to the predicted docking pose, allowing the oxadiazole to pack into a slightly larger hydrophobic pocket.

Our docking campaign also allowed us to obtain further insight into the SAR of **GSK180736A** derivatives. The most favorable and best predicted analogues for GRK activity were the direct amide-linked moieties, likely due to the fact that the two crystal structures used as receptors for the docking campaign were crystallized with ligands that also have a direct amide-linker. Tertiary amides were better tolerated in the methylene- and ethylene-linked compounds likely because the added length of the linkers allowed the amide bond to project further into the hydrophobic subsite or, if there is a clash, out into solvent. Generally, addition of large lipophilic appendages was unfavorable and resulted in a decrease in potency except for cases where there was a basic nitrogen that may have contributed to improved water solubility.

Our screening results also showed that there is little apparent correlation between the docking score (S) and the potency of inhibition exhibited by the selected compounds. We thus carried out additional docking of all forty compounds allowing both the ligand and kinase to be flexible (Supplementary Table 2). Flexible docking was able to better reproduce the crystal structure of GRK2–Gβγ·**33**; however, this second set of flexible docking scores still did not correlate well with the IC_{50} values. This likely reflects the fact that kinases are known to be highly flexible and it is difficult to predict the movement of the surrounding elements of the GRK active site. Additionally, as is well accepted in the computational chemistry community, docking scores are notoriously poor at quantitatively predicting binding affinities. Rather docking is useful for qualitative binding pose generation and compound prioritization for synthesis.

Please cite this article in press as: Waldschmidt H.V., et al. Bioorg. Med. Chem. Lett. (2018), https://doi.org/10.1016/j.bmcl.2018.03.082

Table 3
GRK activity of indazole – dihydropyrimidinone based compounds predicted to be potent against both GRK2 and GRK5.

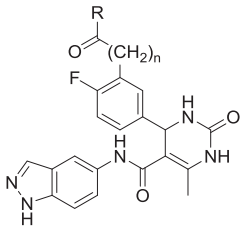

Compound	R	n	GRK2 (IC_{50} μM)	GRK1 (IC_{50} μM)	GRK5 (IC_{50} μM)	GRK2 S	GRK5 S
31	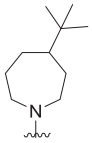	1	3.5 ± 0.7	>100	>100	−8.0	−9.7
32	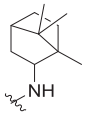	0	4.6 ± 1	>100	>100	−8.1	−9.4
33	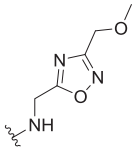	0	0.25 ± 0.07	30 ± 20	0.26 ± 0.2	−9.3	−10.9
34	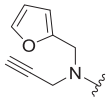	1	0.92 ± 0.1	>100	3.5 ± 0.8	−9.6	−11.0
35	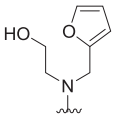	1	0.46 ± 0.08	26 ± 10	1.7 ± 0.3	−10.3	−9.3
36	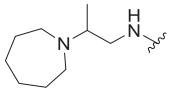	0	1.2 ± 0.7	>100	71 ± 20	−10.5	−9.6
37	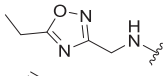	0	0.16 ± 0.07	3.0 ± 0.4	0.38 ± 0.2	−9.7	−11.0
38	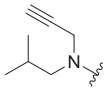	1	2.4 ± 0.5	>100	13 ± 7	−9.8	−11.0
39	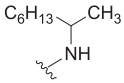	0	4.1 ± 2.5	>100	77 ± 30	−9.8	−11.2
40	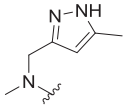	0	1.1 ± 0.1	>100	44 ± 8	−10.4	−9.8
41	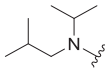	2	12 ± 5	>100	>100	−10.5	−9.8
42	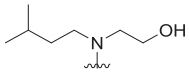	1	1.5 ± 0.40	>100	16 ± 6.1	−10.0	−11.0
43	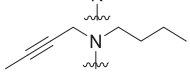	1	0.43 ± 0.2	>100	2.4 ± 0.4	−10.0	−11.0
44	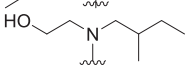	1	0.83 ± 0.3	>100	9.3 ± 4	−10.1	−11.0
45	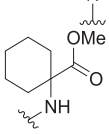	0	0.16 ± 0.2	83 ± 20	19 ± 3	−10.4	−10.1

(*continued on next page*)

Table 3 (*continued*)

Compound	R	n	GRK2 (IC_{50} μM)	GRK1 (IC_{50} μM)	GRK5 (IC_{50} μM)	GRK2 S	GRK5 S
46	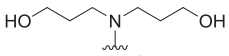	1	0.75 ± 0.05	>100	21 ± 4	−10.6	−10.6
47	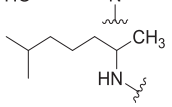	0	4.1 ± 0.9	>100	>100	−10.7	−11.2
48	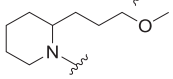	0	29 ± 20	>100	>100	−10.8	−11.0

*All IC_{50} measurements are an average of three separate experiments run in duplicate. Errors shown represent standard error of the mean. S is the docking score generated by MOE.

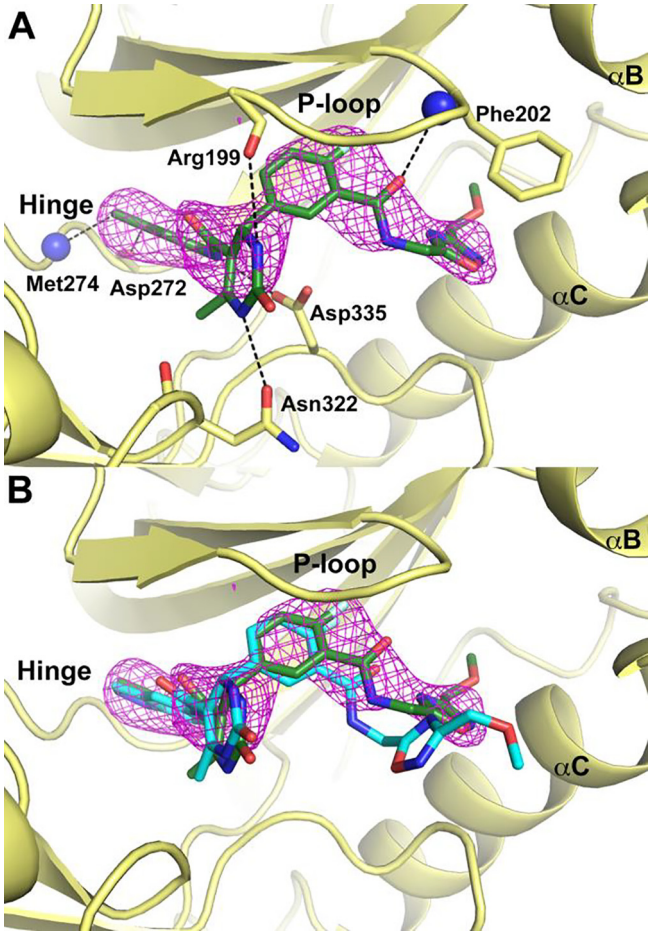

Fig. 5. Comparison of the GRK2–Gβγ·**33** (PDB: 6C2Y) crystal structure and its predicted pose. A) The crystal complex is shown with **33** in dark green. Hydrogen bonds are shown as black dashes and the 3σ omit map is shown as a magenta mesh. B) The docked (cyan) and the crystal (green) poses overlaid.

Nonetheless, our *in silico* screening was successful at identifying two new compounds that showed high potency against both GRK2 and GRK5 (**33** and **37**). Inhibiting GRK2 and GRK5 simultaneously may prove advantageous in treating heart failure, as it would inhibit multiple processes implicated in this disease via both GPCR related and unrelated mechanisms.[4,8] However, we were unable to discover any compounds that displayed high GRK5 selectivity. This may be due to the fact that the lead **GSK180736A** compound already has intrinsic GRK2 selectivity over GRK5 (>130-fold) and that GRK5 has a smaller, more restrictive hydrophobic subsite. Thus, we had the difficult task of trying to build in potency for GRK5 while simultaneously attempting to reduce potency for GRK2 without altering the core of the scaffold responsible for the bulk of binding energy. This challenge is further evident in the fact that of the forty initial most potent compounds predicted by docking/scoring, only five were predicted to bind selectively to GRK5 while seventeen were predicted to bind selectively to GRK2. Moving forward with this particular series of compounds, it seems promising to further investigate the oxadiazole, isoxazole, and pyrazole compounds with direct amide-linkages to further improve GRK5 potency, perhaps in parallel with altering features of the core of the **GSK180736A** scaffold.

Declaration of interest

None.

Acknowledgements

This work was supported by NIH grants HL071818, and HL122416 (to J.T.), and American Heart Association grant 15PRE22730028 (to H.V.W.). J.T. and S.D.L. were supported by grants from the Center for Discovery of New Medicine, University of Michigan. Use of the Advanced Photon Source was supported by the U. S. Department of Energy, Office of Science, Office of Basic Energy Sciences, under Contract No. DE-AC02-06CH11357, and use of LS-CAT Sector 21 was supported by the Michigan Economic Development Corporation and Michigan Technology Tri-Corridor Grant [085P1000817].

A. Supplementary data

Supplementary data associated with this article can be found, in the online version, at https://doi.org/10.1016/j.bmcl.2018.03.082.

References

1. Suo WZ, Li L. Dysfunction of G Protein-Coupled Receptor Kinases in Alzheimer"s Disease. *Sci World J*. 2010;10.
2. Guccione M, Ettari R, Taliani S, Da Settimo F, Zappalà M, Grasso S. G-protein-coupled receptor kinase 2 (GRK2) inhibitors: current trends and future perspectives. *J Med Chem*. 2016;59:9277–9294.
3. Rockman HA, Koch WJ, Lefkowitz RJ. Seven-transmembrane-spanning receptors and heart function. *Nature*. 2002;415:206–212.
4. Huang ZM, Gold JI, Koch WJ. G protein-coupled receptor kinases in normal and failing myocardium. *Front Biosci Landmark*. 2011;16:3047–3060.
5. Anastasios L, Giuseppe R, Walter JK. GRK2 inhibition in heart failure: something old, something new. *Curr Pharm Des*. 2012;18:186–191.
6. Eschenhagen T. Beta-adrenergic signaling in heart failure – adapt or die. *Nat Med*. 2008;14:485–487.
7. Hullmann J, Traynham CJ, Coleman RC, Koch WJ. The expanding GRK interactome: Implications in cardiovascular disease and potential for therapeutic development. *Pharmacol Res*. 2016;110:52–64.
8. Gold JI, Gao E, Shang X, Premont RT, Koch WJ. Determining the absolute requirement of G protein-coupled receptor kinase 5 for pathological cardiac hypertrophy: short communication. *Circ Res*. 2012;111:1048–1053.
9. Rockman HA, Choi DJ, Rahman NU, Akhter SA, Lefkowitz RJ, Koch WJ. Receptor-specific in vivo desensitization by the G protein-coupled receptor kinase-5 in transgenic mice. *Proc Natl Acad Sci*. 1996;93:9954–9959.

10. Ciccarelli M, Chuprun JK, Rengo G, et al. G protein-coupled receptor kinase 2 activity impairs cardiac glucose uptake and promotes insulin resistance after myocardial ischemia. *Circulation*. 2011;123. 1953-U245.
11. Martini JS, Raake P, Vinge LE, et al. Uncovering G protein-coupled receptor kinase-5 as a histone deacetylase kinase in the nucleus of cardiomyocytes. *Proc Natl Acad Sci*. 2008;105:12457–12462.
12. Homan KT, Larimore KM, Elkins JM, Szklarz M, Knapp S, Tesmer JJG. Identification and Structure-Function Analysis of Subfamily Selective G Protein-Coupled Receptor Kinase Inhibitors. *ACS Chem Biol*. 2014;10:310–319.
13. Waldschmidt HV, Homan KT, Cruz-Rodríguez O, et al. Structure-based design, synthesis, and biological evaluation of highly selective and potent G protein-coupled receptor kinase 2 inhibitors. *J Med Chem*. 2016;59:3793–3807.
14. Johnson LR, Scott MGH, Pitcher JA. G protein-coupled receptor kinase 5 contains a DNA-binding nuclear localization sequence. *Mol Cell Biol*. 2004;24:10169–10179.
15. Yi YP, Gerdes AM, Li FQ. Myocyte redistribution of GRK2 and GRK5 in hypertensive, heart-failure-prone rats. *Hypertension*. 2002;39:1058–1063.
16. McKinsey TA, Olson EN. Toward transcriptional therapies for the failing heart: chemical screens to modulate genes. *J Clin Invest*. 2005;115:538–546.
17. Chang SR, McKinsey TA, Zhang CL, Richardson JA, Hill JA, Olson EN. Histone deacetylases 5 and 9 govern responsiveness of the heart to a subset of stress signals and play redundant roles in heart development. *Mol Cell Biol*. 2004;24:8467–8476.
18. Obrenovich ME, Palacios HH, Gasimov E, Leszek J, Aliev G. The GRK2 overexpression is a primary hallmark of mitochondrial lesions during early alzheimer disease. *Cardiovasc Psychiatry Neurol*. 2009;2009:327360.
19. Er B, Vv G, Jn J, Jl B, Ev G. Arrestins and two receptor kinases are upregulated in Parkinson's disease with dementia. *Neurobiol Aging*. 2008;29:379–396.
20. Wu C-C, Tsai F-M, Shyu R-Y, Tsai Y-M, Wang C-H, Jiang S-Y. G protein-coupled receptor kinase 5 mediates Tazarotene-induced gene 1-induced growth suppression of human colon cancer cells. *BMC Cancer*. 2011;11. 175-175.
21. Métayé T, Menet E, Guilhot Jl, Kraimps J-L. Expression and activity of g protein-coupled receptor kinases in differentiated thyroid carcinoma. *J Clin Endocrinol Metab*. 2002;87:3279–3286.
22. Geras-Raaka E, Arvanitakis L, Bais C, Cesarman E, Mesri EA, Gershengorn MC. Inhibition of constitutive signaling of kaposi's sarcoma–associated herpesvirus G protein-coupled receptor by protein kinases in mammalian cells in culture. *J Exp Med*. 1998;187:801–806.
23. Kim JI, Chakraborty P, Wang Z, Daaka Y. G-protein coupled receptor kinase 5 regulates prostate tumor growth. *J Urol*. 2012;187:322–329.
24. Wang F-L, Tang L-Q, Wei W. The connection between GRKs and various signaling pathways involved in diabetic nephropathy. *Mol Biol Rep*. 2012;39:7717–7726.
25. Li H, Gan W, Lu L, et al. A genome-wide association study identifies GRK5 and RASGRP1as Type 2 diabetes loci in chinese hans. *Diabetes*. 2013;62:291–298.
26. Cho SY, Lee BH, Jung H, et al. Design and synthesis of novel 3-(benzo[d]oxazol-2-yl)-5-(1-(piperidin-4-yl)-1H-pyrazol-4-yl)pyridin-2-amine derivatives as selective G-protein-coupled receptor kinase-2 and -5 inhibitors. *Bioorg Med Chem Lett*. 2013;23:6711–6716.
27. Lee J, Han S-Y, Jung H, et al. Synthesis and structure–activity relationship of aminopyridines with substituted benzoxazoles as c-Met kinase inhibitors. *Bioorg Med Chem Lett*. 2012;22:4044–4048.
28. Homan KT, Wu E, Wilson MW, Singh P, Larsen SD, Tesmer JJG. Structural and functional analysis of G protein-coupled receptor kinase inhibition by paroxetine and a rationally designed analog. *Mol Pharmacol*. 2014;85:237–248.
29. Homan KT, Waldschmidt HV, Glukhova A, et al. Crystal structure of G protein-coupled receptor kinase 5 in complex with a rationally designed inhibitor. *J Biol Chem*. 2015.
30. Molecular Operating Environment (MOE), Chemical Computing Group ULC: 1010 Sherbooke St. West, Suite #910, Montreal, QC, Canada, H3A 2R7, 2017.
31. Sridharan V, Ruiz M, Menéndez JC. Mild and high-yielding synthesis of β-keto esters and β-ketoamides. *Synthesis*. 2010;2010:1053–1057.
32. Drewry DHE, Brian; Goodman, Krista B, Green, Darren, Victor, Steven, Jung, David, Kendall; Lee, Denis; Stavenger, Robert A, Wad, Sjoerd, Nocolaas Chemical Compounds. 29 December 2004, 2004.
33. Homan KT, Tesmer JJG. Molecular basis for small molecule inhibition of G protein-coupled receptor kinases. *ACS Chem Biol*. 2015;10:246–256.